



Mechanical and corrosion properties of Ti–35Nb–7Zr–*x*HA composites fabricated by spark plasma sintering

Zheng-yuan HE¹, Lei ZHANG¹, Wen-rui SHAN¹, Yu-qin ZHANG^{1,2}, Rong ZHOU¹, Ye-hua JIANG¹, Jun TAN^{1,3,4}

1. School of Materials Science and Engineering,

Kunming University of Science and Technology, Kunming 650093, China;

2. Engineering Technology Research Center of Titanium Products and Application of Yunnan Province,
Kunming 650093, China;

3. Institute for Complex Materials, IFW Dresden, Dresden D-01171, Germany;

4. Institute of Materials Science, TU Dresden, Dresden D-01062, Germany

Received 31 January 2016; accepted 7 July 2016

Abstract: To improve the bioactivity of Ti–Nb–Zr alloy, Ti–35Nb–7Zr–*x*HA (hydroxyapatite, *x*=5, 10, 15 and 20, mass fraction, %) composites were fabricated by spark plasma sintering. The effects of the HA content on microstructure, mechanical and corrosion properties of the composites were investigated utilizing X-ray diffraction (XRD), scanning electron microscope (SEM), mechanical tests and electrochemical tests. Results show that all sintered composites are mainly composed of β -Ti matrix, α -Ti and metal–ceramic phases (CaO, CaTiO₃, CaZrO₃, Ti_{*x*}P_{*y*}, etc). Besides, some residual hydroxyapatites emerge in the composites (15% and 20% HA). The compressive strengths of the composites are over 1400 MPa and the elastic moduli of composites ((5%–15%) HA) present appropriate values (46–52 GPa) close to that of human bones. The composite with 15% HA exhibits low corrosion current density and passive current density in Hank's solution by electrochemical test, indicating good corrosion properties. Therefore, Ti–35Nb–7Zr–15HA composite might be an alternative material for orthopedic implant applications.

Key words: titanium composite; spark plasma sintering; microstructure; mechanical properties; corrosion properties

1 Introduction

Pure Ti and Ti–6Al–4V alloy are the most common biomaterials for implants due to their outstanding characteristics such as high specific strength, excellent corrosion resistance, good biocompatibility, complete inertness to the body environment, low modulus and wonderful capacity to join with bones and tissues [1–3]. Low modulus and high corrosion resistance are prime requirements for the longevity of implant materials. However, the elastic moduli of pure Ti and Ti–6Al–4V alloy (110 GPa) are much higher than that of human bones (10–30 GPa) [4]. The elastic modulus mismatch would cause bone loss, implant loosening and premature failure of artificial hip [5]. Therefore, it is very important to choose biomaterials whose moduli are close to that of human bones. β type Ti–Nb–Zr alloys with low elastic

modulus and excellent corrosion resistance are regarded as one of the most promising alloys in biomedical applications [6–9]. Recently, Ti–35Nb–7Zr alloy with the elastic modulus of about 54 GPa possesses favorable mechanical properties [10]. However, almost all metallic biomaterials, including Ti–35Nb–7Zr alloy, are bio-inert. These biomaterials cannot effectively interact with surrounding bone tissues while they are used as implants. Hydroxyapatite (HA) has similar composition and structure to human bones so that it has excellent biocompatibility with human bones [11,12]. The bio-ceramic has been used clinically for both dental and orthopedic implants. Nevertheless, its application in load-bearing implants is limited owing to its poor mechanical properties [13]. Ti-based/bio-ceramic composites have attracted considerable attention for biomedical implant application because of the superior properties of pure Ti or Ti alloy and the wonderful

chemical bonding ability of bio-ceramic (e.g., as HA-hydroxyapatite) to bones [14,15]. Traditionally, the ceramic is coated on Ti-based alloys to improve the biocompatibility of the alloys by surface modification methods [16–18]. But the differences in physical properties between Ti-based alloys and bio-ceramic would cause many problems, such as the coating layer peeled off, the surface crack, low interface strength between matrix and surface layer. Spark plasma sintering (SPS) technique is a good way of metallurgic and sintering method. Therefore, for sake of overcoming the above mentioned problems, SPS technique is implemented to fabricate Ti-based/bio-ceramic composite [19,20]. Current studies report that some excellent Ti–Nb–Zr–HA composites could be fabricated by SPS technique [21]. The results show that the sintered Ti–35%Nb–7%Zr–10%HA composite has high hardness and high bioactivity with increased milling time, but at the cost of the sintering ability. However, the influence of HA contents on mechanical properties (strength and elastic modulus) and electrochemical characterization of Ti–35Nb–7Zr–HA composites is not mentioned.

In this work, Ti–35Nb–7Zr– x HA ($x=5, 10, 15, 20$, mass fraction, %) composites were successfully fabricated by SPS at 1050 °C. The aim of this work was to investigate the effects of HA content on relative density, microstructure, mechanical and corrosion properties of sintered composites. It was expected to obtain a implant material with low modulus, high strength and enhanced bioactivity by combining Ti–35Nb–7Zr alloy with HA bio-ceramic.

2 Experimental

The characteristics of the pure initial Ti, Nb, Zr and HA powders were presented in Table 1. The raw powders were prepared according to the nominal composition of Ti–35Nb–7Zr alloy and Ti–35Nb–7Zr– x HA composites ($x=5, 10, 15, 20$). The milling process was conducted in a mill/mixer machine (XQM–4) with sealed stainless steel container and balls under vacuum atmosphere, and the mass ratio of balls to powder was 3:1. At first, the Ti–Nb–Zr powders were milled for 10 h, and then HA powders were added into Ti–Nb–Zr powers for further mixing for 2 h. During the 10 h milling and 2 h mixing process, anhydrous alcohol was used to avoid cold welding and polluting among powders. The blended powders were dried and loaded into the cylindrical graphite die (outside diameter: 30 mm, inside diameter: 20 mm and height: 40 mm). The sintering process was carried on SPS–515S at 1050 °C in a vacuum chamber of 5–10 Pa, under a uniaxial pressure of 40 MPa. The heating rate and holding time were 100 °C/min and 5 min, respectively. Sintering temperature was measured

using a pyrometer focused on the surface of the graphite die. The sintered samples were then cooled to room temperature inside the furnace. When the temperature was lower than 100 °C, the sintered samples were taken out of the die. Then, the sintered samples were subsequently ground and polished to obtain fine and graphite-free surfaces.

Table 1 Characteristics of Ti, Nb, Zr and HA powders

Powder	Purity/%	Powder size/ μm
Ti	99.50	25
Nb	99.95	10.5
Zr	99.50	25
HA	99.99	0.1

The phases of the sintered samples were investigated using X-ray diffraction (XRD) (Bruker, D8 Advance, Germany) with Cu K_{α} radiation within the range of 20°–80°. The morphology of Ti–35Nb–7Zr– x HA composites was observed by scanning electron microscope (FEI, QUAN 600, Netherlands). The density of samples was calculated by Archimedes' method. The mechanical properties of the sintered samples were tested by universal testing machine (Shimadzu, AG-X 100 KN, Japan). The samples were processed into d_4 mm \times 10 mm and d_2 mm \times 10 mm for measuring compressive strength and compressive elastic modulus, respectively. The compression rate in the test was 1 mm/min.

Electrochemical tests were investigated by Tafel and anodic polarization techniques in Hank's solution at 37 °C. The corrosion tests were conducted using electrochemical workstation (Bio-Logic, SAS SP300, France). The chemical composition of Hank's solution contained NaCl 8 g/L, glucose 1 g/L, NaHCO₃ 0.35 g/L, KCl 0.4 g/L, CaCl₂ 0.14 g/L, MgCl₂·6H₂O 0.1 g/L, KH₂PO₄ 0.06 g/L, Na₂HPO₄·2H₂O 0.06 g/L, and MgSO₄·7H₂O 0.06 g/L [22], and the pH value of the simulated body fluid solution was maintained at 7.4. The reference system was saturated calomel electrode (SCE). A platinum electrode was used as counter electrode and the tested sample with 1 cm² was used as working electrode. Anodic polarization curves were measured from –1.5 to 1.5 V (SCE) with a scanning rate of 5 mV/s.

3 Results and discussion

3.1 Relative density

Figure 1 shows the relative density of sintered samples. It was notable that the relative density of composites was lower than that of Ti–35Nb–7Zr alloy (99.5%). With increasing HA content from 5% to 20%, the relative density decreased from 99.0% to 96.2%. This phenomenon could be related to the HA addition.

Nevertheless, the relative density was higher than that of counterparts with 10% HA [21], because increasing milling time (e.g., 10 h) led to finer particles, thus affecting densification and sintering ability. With increasing HA content, the porosity of composites enhanced because the HA ceramic decreased the SPS sintering ability, which led to lower relative density in the composites. However, it was harmful to their mechanical properties if the densification in composites was decreased. Therefore, it was very necessary to control the HA content within an optimum range.

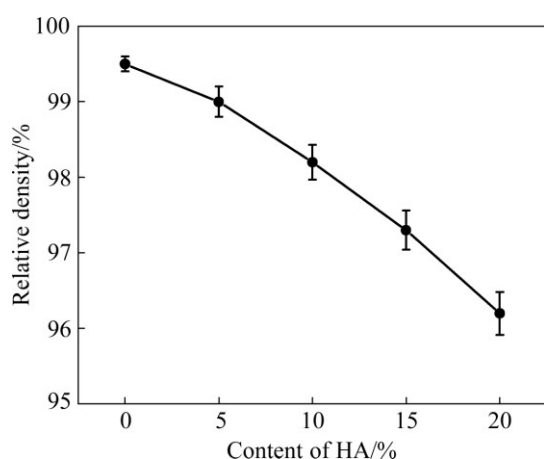


Fig. 1 Relative density of sintered Ti-35Nb-7Zr alloy and Ti-35Nb-7Zr-xHA composites ($x=5, 10, 15, 20$) at 1050 °C

3.2 Microstructure

To elucidate the effect of sintering process on phase formation, the XRD analysis was conducted on sintered Ti-35Nb-7Zr alloy and Ti-35Nb-7Zr-xHA composites, and the results are shown in Fig. 2. It could be seen that the Ti-35Nb-7Zr alloy mainly consisted of β -Ti matrix and the Ti-35Nb-7Zr-xHA composites ($x=5$ and 10) consisted of β matrix, a little α -Ti phases, and some reaction products (i.e., CaTiO₃, CaO, CaZrO₃, Ti_xP_y). Nevertheless, some residual HAs emerged in the

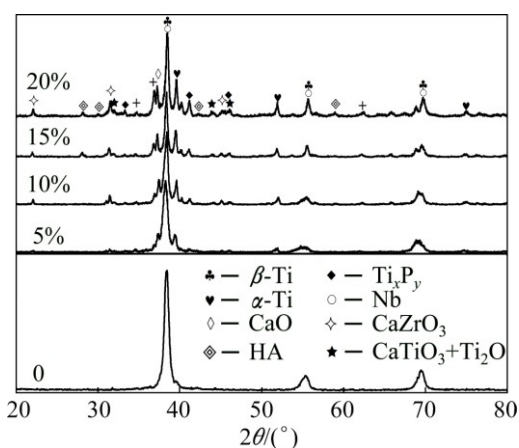
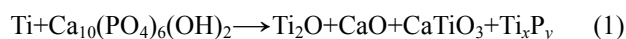


Fig. 2 XRD patterns of sintered Ti-35Nb-7Zr alloy and Ti-35Nb-7Zr-xHA composites ($x=5, 10, 15, 20$) at 1050 °C

composites with 15% and 20% HA. It was notable that α -Ti phase still remained in all sintered samples, except for Ti-35Nb-7Zr alloy.

When the addition of HA varied from 5% to 20%, the α -Ti peaks became stronger, especially in composite with 20% HA. This was because more HA powders presented around the Ti powders and β -Ti stabilization elements (e.g., Nb and Zr), the intensity of diffusion among Ti, Nb and Zr elements during sintering was decreased. Thus, the transformation from α to β phase could be hindered. In other words, the amount of α -Ti phase increased due to the hindering effects of HA during the process of diffusion for β -Ti stabilisation elements. In fact, the interstitial α -stabilizer (e.g., O) decomposed from HA might hindered the transformation from α to β phase. Therefore, the fraction of α -Ti phase in Ti-35Nb-7Zr-xHA composites increased with increasing HA content, which could lead to the increase of elastic properties because α -Ti had high elastic modulus.

In addition, the XRD patterns showed reaction products (metal-ceramic phases) such as: Ti₂O, CaO, CaTiO₃, CaZrO₃, and Ti_xP_y, which formed in composites during sintering. The metal-ceramic phases could be formed through the following possible reactions as expressed in Eqs. (1) – (3) [21,23,24]:



The results above suggested that the phase composition of sintered Ti-35Nb-7Zr-xHA composites was affected by HA content. Too much HA could not only increase the population of metal-ceramic phases but also result in some residual HA in the composites with 15% and 20% HA due to incomplete reaction between the metal elements and the ceramic. These metal-ceramic phases might be strengthening phases which raised the strength and elastic modulus of sintered composites.

Figure 3 shows SEM images of sintered Ti-35Nb-7Zr alloy and Ti-35Nb-7Zr-xHA composites. One could see that the Ti-35Nb-7Zr alloy was mainly composed of Ti-rich regions and Nb-rich regions. The Ti-rich regions and Nb-rich regions appeared to be dark-grey or grey and white, respectively (Fig. 3(a)). When 5% HA was added, the grain sizes of Ti-rich regions and Nb-rich regions decreased, and the small holes appeared. The sintering reaction products could be observed around the grain boundary, marked as the arrow in Fig. 3(b). More HA additions introduced more holes and smaller grains, as shown in Fig. 3(c). When the HA content was more than 10%, continuous net-like structures could be observed in the Ti matrix, as shown

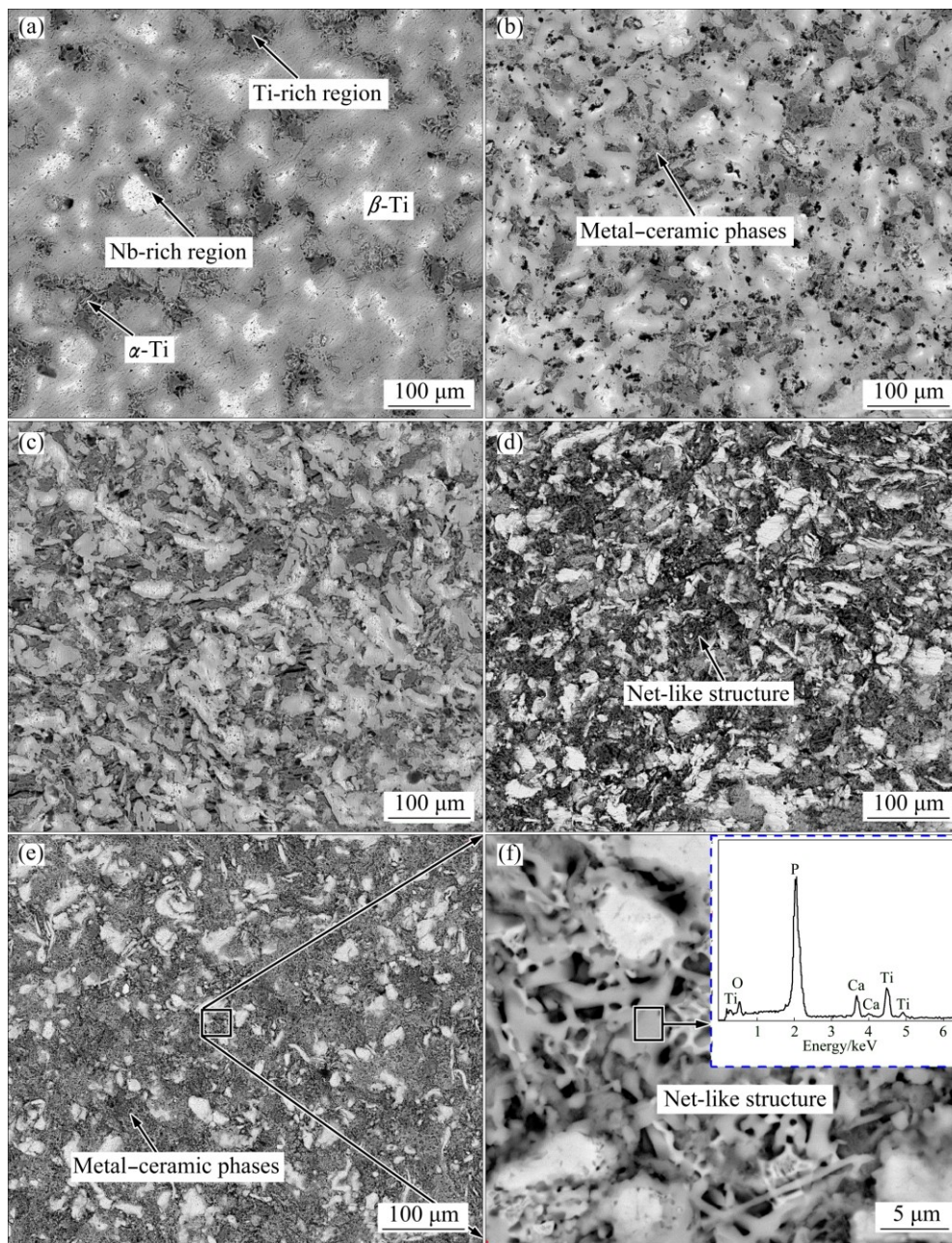


Fig. 3 SEM images of Ti-35Nb-7Zr alloy (a), Ti-35Nb-7Zr-5HA composite (b), Ti-35Nb-7Zr-10HA composite (c), Ti-35Nb-7Zr-15HA composite (d), Ti-35Nb-7Zr-20HA composite (e, f)

in Figs. 3(d) and (e), and a local magnification view (Fig. 3(f)), which gave rise to much finer grains. The net-like structures consisted of Ti, Ca, P and O elements identified by EDS, as shown in Fig. 3(f). Therefore, it could be inferred that metal-ceramic phases exhibited net-like distribution with HA content exceeding 10%.

Tiny holes in the composites increased due to the difference of thermal expansion coefficient between the ceramic and the metal. Thus, the porosity increased with the increase of HA content, causing lower relative density, as described in Fig. 1. However, the finer grains were in favor of compressive strength of the composites. Furthermore, the X-ray mapping images of sintered

composites, taking Ti-35Nb-7Zr-10HA and Ti-35Nb-7Zr-15HA at 1050 °C as examples, illustrated that partial Ca and P would gather in the holes, because the compounds with partial Ca and P were precipitated around Ti matrix during cooling process, marked as the arrows in Fig. 4(a). However, there were a large amount of P elements diffused into the Ti matrix, marked as the circles in Fig. 4(b). Hence, when the HA content exceeded 10%, the metal-ceramic phases presented homogeneous and continuous distribution around or upon the matrix. As we know that Ca and P are the main elements of HA. A certain Ca and P would improve the bioactivity of Ti alloys.

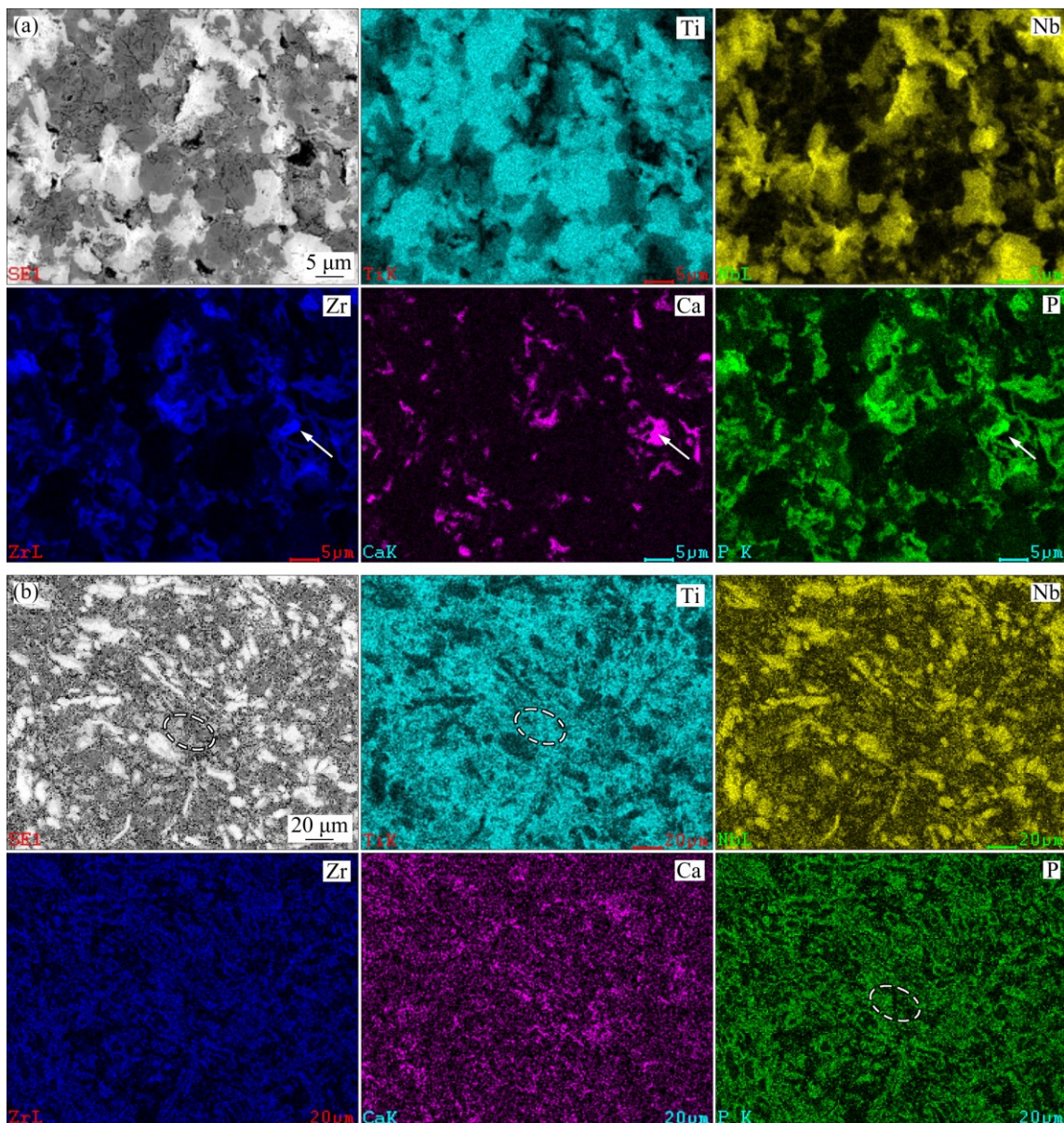


Fig. 4 X-ray mapping images of Ti-35Nb-7Zr-xHA composites: (a) $x = 10$, (b) $x = 15$

According to the sintering reaction mentioned above, these elements, like Ca and P, would exist as metal-ceramic phases, which could have a significant influence on the performance of composites. Meanwhile, the holes existing on the surface of composites would be beneficial to the induction of osteocyte growth, but would be harmful to mechanical properties.

3.3 Mechanical properties

Compressive strain-stress curves of Ti-35Nb-7Zr alloy and Ti-35Nb-7Zr-xHA composites are shown in Fig. 5. When the HA addition was more than 5%, there was no obvious yielding band stage in the strain-stress curves and only elastic fracture behavior appeared in all composites. The main reason for early failure behaviors of the composites was the change of microstructure when

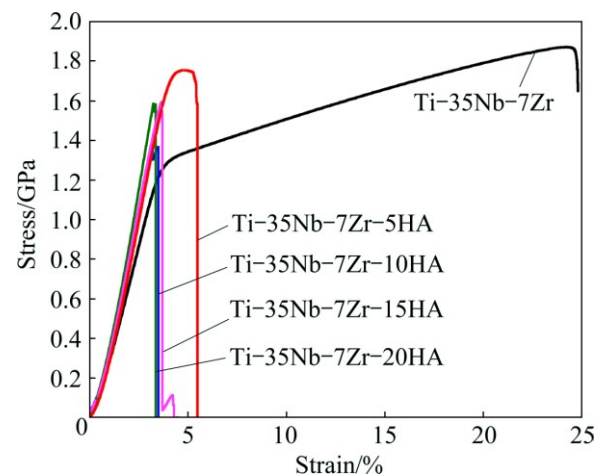


Fig. 5 Compressive strain-stress curves of Ti-35Nb-7Zr alloy and Ti-35Nb-7Zr-xHA composites ($x = 5, 10, 15, 20$)

the HA was added. Lots of holes and metal–ceramic phases in composite were engendered by HA addition.

Figure 6 shows the compressive elastic modulus and compressive strength of Ti–35Nb–7Zr alloy and Ti–35Nb–7Zr–*x*HA composites. It could be seen from Fig. 6 that the HA addition had a significant effect on mechanical behaviors of the composites. The Ti–35Nb–7Zr alloy had an average compressive strength of about 1990 MPa. With increasing HA content, the average compressive strength of Ti–35Nb–7Zr–*x*HA composites decreased and then slightly increased, which was lower than that of Ti–35Nb–7Zr alloy (1990 MPa). The average compressive strength decreased from 1850 to 1405 MPa when the HA content varied from 5% to 10%. However, when the HA content was 15% and 20%, the average compressive strength of the sintered composites increased to 1600 and 1630 MPa, respectively. The most important reason for the foresaid phenomenon could be attributed to the numerous net-like phases, which continuously distributed in Ti matrix, which could play an more important role than holes when HA content exceeded 10%. The net-like phases (as shown in Fig. 3) could improve the whole quality and thus increase the compressive strength. Therefore, the composites with 15% and 20% HA exhibited higher compressive strength compared with Ti–35Nb–7Zr–10HA. Furthermore, it should be mentioned that the compressive strength of Ti–35Nb–7Zr–15HA and Ti–35Nb–7Zr–20HA composites were slightly lower than that of ultrafine-grained TC4 alloy (1663 MPa) fabricated by sparking plasma sintering [25] and significantly higher than that of ultrafine-grained Ti (1100 MPa) [26], thus meeting the requirements of biomedical implant design. Contrary to the tendency of the strength, the average compressive elastic moduli of the sintered samples consistently increased from 43 to 65 GPa with increasing HA content from 0 to 20%. It was noteworthy that the average elastic moduli of the

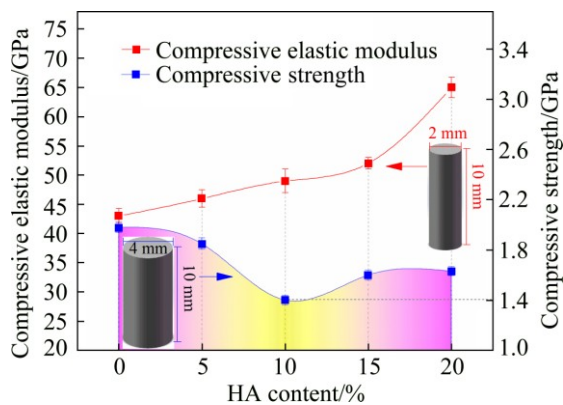


Fig. 6 Compressive elastic modulus and compressive strength of Ti–35Nb–7Zr alloy and Ti–35Nb–7Zr–*x*HA composites (*x*=5, 10, 15, 20)

composites increased significantly from 49 GPa (for 10% HA) and 52 GPa (for 15% HA) to 65 GPa when HA content exceeded 15% due to the increase of the metal–ceramic phases and residual HA phase. The sintered HA had a high elastic modulus of about 111 GPa [27], so the metal–ceramic phases could also be hard phases. These could cause high elastic modulus of the composite, which could result in “stress shielding” as an implant material. Therefore, the elastic modulus of composites with 5%, 10% and 15% HA varied from 46 to 52 GPa, which was slightly higher than that of the Ti–35Nb–7Zr alloy (43 GPa) and some Ti–Nb–Zr based biomedical alloys (e.g., TiNbZrTaSi alloy [28], Ti_{65.5}Nb_{22.3}Zr_{4.6}Ta_{1.6}Fe₆ alloy [29]) fabricated by SPS, indicating a favorable mechanical compatibility.

3.4 Corrosion properties

The anodic polarization curves of Ti–35Nb–7Zr alloy and Ti–35Nb–7Zr–*x*HA composites in Hank’s solution (pH=7.4) at 37 °C are shown in Fig. 7. The inset in the figure highlighted the anodic polarization curves in the range from 0.3 to 1.5 V (vs SCE). The corrosion current densities (J_{corr}) and corrosion potential (ϕ_{corr}) were obtained from the polarization curves by Tafel plots using both cathodic and anodic branches of the polarization on curves. Table 2 summarized the corrosion parameters for samples in Hank’s solution at 37 °C. With the increase of HA content, the ϕ_{corr} values of bulk composites in the Hank’s solution decreased, but the J_{corr} values of bulk composites increased and then decreased. The J_{corr} of the composites was higher than that of Ti–35Nb–7Zr alloy. When the HA content varied from 5% to 10%, the J_{corr} changed from 1.370 to 2.368 μA . With HA content exceeding 10%, the J_{corr} of composites decreased drastically from 2.368 μA to 1.482 μA (for 15% HA) and 1.463 μA (for 20% HA). However, the J_{corr} of all composites was lower than that of the cold sprayed 20% HA/Ti composite (J_{corr} =3.67 $\mu\text{A}/\text{cm}^2$) [30]. It was

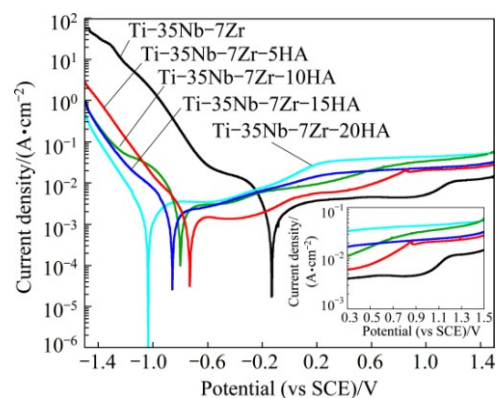


Fig. 7 Anodic polarization curves of Ti–35Nb–7Zr alloy and Ti–35Nb–7Zr–*x*HA composites (*x*=5, 10, 15, 20) in Hank’s solution (pH = 7.4) at 37 °C

Table 2 Corrosion parameter values of Ti–35Nb–7Zr alloy and Ti–35Nb–7Zr–*x*HA composites (*x*=5, 10, 15, 20) in Hank's solutions (pH = 7.4) at 37 °C

Sintered composite	φ_{corr} (vs SCE)/V	J_{corr} ($\mu\text{A}\cdot\text{cm}^{-2}$)
Ti–35Nb–7Zr	–0.135	1.106
Ti–35Nb–7Zr–5HA	–0.723	1.370
Ti–35Nb–7Zr–10HA	–0.756	2.368
Ti–35Nb–7Zr–15HA	–0.840	1.482
Ti–35Nb–7Zr–20HA	–1.047	1.463

notable that the J_{corr} of Ti–35Nb–7Zr–15HA composite was quite approximate to those of Ti–35Nb–7Zr–5HA composite and Ti–35Nb–7Zr alloy, exhibiting similar corrosion resistance.

The composites presented different active–passive features. The current density of Ti–35Nb–7Zr–10HA composite increased with the increase of potential, indicating no obvious active–passive transition. The current oscillations observed in the Ti–35Nb–7Zr–10HA composite were generally attributed to the instability of discontinuous metal–ceramic phases and a large amounts of holes. While the anodic polarization curves of the composites, except for Ti–35Nb–7Zr–10HA, showed an obvious active–passive transition. The passive regions of these samples were different owing to different HA contents. The Ti–35Nb–7Zr–15HA and Ti–35Nb–7Zr–20HA composites without significant current oscillations presented passivation between 0.3 V and 1.5 V with the evidence of an active–passive transition, due to coalescence between metal–oxide films and continuously distributed metal–ceramic phases. Nevertheless, the current density of Ti–35Nb–7Zr–5HA composite increased with the increase of potential until approximately 0.88 V, and then the sample was passivated until the end of the test at 1.5 V. This was attributed to more metal–oxides and less holes than that of Ti–35Nb–7Zr–10HA composite. The primary passive current densities in the passive region of Ti–35Nb–7Zr–5HA, Ti–35Nb–7Zr–15HA and Ti–35Nb–7Zr–20HA composites were about 17.2, 18.6 and 34 μA , respectively, which were higher than that of Ti–35Nb–7Zr alloy. Metal would spontaneously be passivated if the critical current density of the metal was less than 100 $\mu\text{A}/\text{cm}^2$ [31]. So, it could be seen that the polarization behavior might be regarded as stable passivity.

Analyses on the reason, it was interesting that both corrosion and passive behaviors were attributed to HA addition. In the case of Ti–Nb–Zr alloy, Ti solid solution alloying with Nb, Zr could provide some passivity even under conditions where the metal–oxides (such as TiO_2 and Nb_2O_5) have been dissolved [32]. But the corrosion

behavior of Ti–35Nb–7Zr–HA composite was strongly dependent on surface appearances, metal–oxides and metal–ceramic phases. The J_{corr} increased with HA content varied from 5% to 10% because a lot of holes on the composite surface were engendered by HA addition and the metal–ceramic phases were discontinuous. The amount of holes increased the corrosion area, and the surface of composites was easily corroded along flaw in the holes during corrosion process. However, when the HA content exceeded 10%, the numerous net-like phases (metal–ceramic phases), continuously distributing in Ti matrix, could play an more important role than holes. The net-like phases combining with Ti or Nb solid solution resisted the corrosion in Hank's solution. Therefore, the composites with 15% and 20% HA addition exhibited depressed J_{corr} and stable passivation regions. Furthermore, the variation for the J_{corr} of composites could be attributed to the potential difference between the matrix and the metal–ceramic phases [33].

In a word, it was clear that moderate HA addition (15%) in Ti–Nb–Zr alloy was helpful to obtain good corrosion resistance. The composite with 15% HA had lower passive current density than Ti–35Nb–7Zr–20HA composite and similar corrosion current density to that of Ti–35Nb–7Zr–5HA composite, which exhibited excellent electrochemical properties in human body environment. Therefore, more bio-ceramic with good corrosion property, better modulus property and moderate strength suggested that the Ti–35Nb–7Zr–15HA composite could be an alternative material in orthopedic implant applications.

4 Conclusions

1) Ti–35Nb–7Zr–*x*HA composites (*x*=5, 10, 15 and 20) mainly consisted of β -Ti matrix, a little α -Ti and metal–ceramic phases such as CaO, CaTiO_3 , CaZrO_3 , Ti_xP_y , and so on. Besides, some residual HA emerged in the composites with 15% and 20% HA.

2) The addition of HA would lead to finer grains of composites. When the HA content exceeded 10%, the metal–ceramic phases presented homogeneous and continuous distribution around or upon the matrix.

3) The elastic modulus of composites varied from 5% to 15% HA presented a smaller variation between 43 GPa and 52 GPa, and the compressive strength could reach 1400 MPa.

4) With the increase of HA content, J_{corr} of composites increased first and then decreased. The Ti–35Nb–7Zr–15HA composite exhibited significantly lower passive current density than Ti–35Nb–7Zr–20HA and similar corrosion current density to that of Ti–35Nb–7Zr–5HA composite.

Acknowledgements

This work is supported by National-local Joint Engineering Laboratory of Metal Advanced Solidification Forming and Equipment Technology of China. We also would like to acknowledge financial support provided by the Analysis and Testing Foundation of Kunming University of Science and Technology (2016T20090120), China.

References

- [1] LI S J, XU Q S, WANG Z, HOU W T, HAO Y L, YANG R, MURR L E. Influence of cell shape on mechanical properties of Ti–6Al–4V meshes fabricated by electron beam melting method [J]. *Acta Biomaterialia*, 2014, 10(10): 4537–4547.
- [2] EISENBARTH E, VELTEN D, MÜLLER M, THULL R, BREME J. Biocompatibility of β -stabilizing elements of titanium alloys [J]. *Biomaterials*, 2004, 25(26): 5705–5713.
- [3] BRUNEEL N, HELSEN J A. In vitro simulation of biocompatibility of Ti–Al–V [J]. *Journal of Biomedical Materials Research*, 1988, 22(3): 203–214.
- [4] CHEN Q Z, THOUAS G A. Metallic implant biomaterials [J]. *Materials Science and Engineering R: Reports*, 2015, 87: 1–57.
- [5] NIINOMI M. Mechanical biocompatibilities of titanium alloys for biomedical applications [J]. *Journal of the Mechanical Behavior of Biomedical Materials*, 2008, 1(1): 30–42.
- [6] MARTINS D Q, SOUZA M E P, SOUZA S A, ANDRADE D C, FREIRE C M A, CARAM R. Solute segregation and its influence on the microstructure and electrochemical behavior of Ti–Nb–Zr alloys [J]. *Journal of Alloys and Compounds*, 2009, 478(1–2): 111–116.
- [7] XU Yan-fei, XIAO Yi-feng, YI Dan-qing, LIU Hui-qun, WU Liang, WEN Jing. Corrosion behavior of Ti–Nb–Ta–Zr–Fe alloy for biomedical applications in Ringer’s solution [J]. *Transactions of Nonferrous Metals Society of China*, 2015, 25(8): 2556–2563.
- [8] MOHAMMED M T, KHAN Z A, GEETHA M. Effect of thermo-mechanical processing on microstructure and electrochemical behavior of Ti–Nb–Zr–V new metastable beta titanium biomedical alloy [J]. *Transactions of Nonferrous Metals Society of China*, 2015, 25(3): 759–769.
- [9] JIN L, CUI Wen-fang, SONG Xiu, LIU Gang, ZHOU Lian. Effects of surface nanocrystallization on corrosion resistance of β -type titanium alloy [J]. *Transactions of Nonferrous Metals Society of China*, 2014, 24(8): 2529–2535.
- [10] CHAVES J M, FLORÊNCIO O, SILVA P S Jr, MARQUES P W B, SCHNEIDER S G. Anelastic relaxation associated to phase transformations and interstitial atoms in the Ti–35Nb–7Zr alloy [J]. *Journal of Alloys and Compounds*, 2014, 616: 420–425.
- [11] MURALITHRAN G, RAMESH S. The effects of sintering temperature on the properties of hydroxyapatite [J]. *Ceramics International*, 2000, 26(2): 221–230.
- [12] DI SILVIO L, BONFIELD W. Biodegradable drug delivery system for the treatment of bone infection and repair [J]. *Journal of Materials Science Materials in Medicine*, 1999, 10(10–11): 653–658.
- [13] GAUTIER S, CHAMPION E, BERNACHE-ASSOLLANT D, CHARTIER T. Rheological characteristics of alumina platelet-hydroxyapatite composite suspensions [J]. *Journal of the European Ceramic Society*, 1999, 19(4): 469–477.
- [14] NING C Q, ZHOU Y. Correlations between the in vitro and in vivo bioactivity of the Ti/HA composites fabricated by a powder metallurgy method [J]. *Acta Biomaterialia*, 2008, 4(6): 1944–1952.
- [15] BOVAND D, YOUSEFPOUR M, RASOULI S, BAGHERIFARD S, BOVAND N, TAMAYOL A. Characterization of Ti–HA composite fabricated by mechanical alloying [J]. *Materials and Design*, 2015, 65: 447–453.
- [16] BODHAK S, BOSE S, BANDYOPADHYAY A. Electrically polarized HAP-coated Ti: In vitro bone cell-material interactions [J]. *Acta Biomaterialia*, 2010, 6(2): 641–651.
- [17] BALOYI N M, POPOOLA A P I, PITAYANA S L. Microstructure, hardness and corrosion properties of laser processed Ti6Al4V-based composites [J]. *Transactions of Nonferrous Metals Society of China*, 2015, 25(9): 2912–2923.
- [18] ZHAO Guo-liang, XIA Long, ZHONG Bo, WU Song-song, SONG Liang, WEN Guang-wu. Effect of alkali treatments on apatite formation of microarc-oxidized coating on titanium alloy surface [J]. *Transactions of Nonferrous Metals Society of China*, 2015, 25(4): 1151–1157.
- [19] WANG Xiao-peng, XU Li-Juan, CHEN Yu-yong, WOO Kee-do, XIAO Shu-long, KONG Fan-tao, LIU Zhi-guang. Effect of milling time on microstructure of Ti35Nb2.5Sn/10HA biocomposite fabricated by powder metallurgy and sintering [J]. *Transactions of Nonferrous Metals Society of China*, 2012, 22(22): 608–612.
- [20] GHESMATI TABRIZI S, BABAKHANI A, SAJJADI S A, LÜ W J. Microstructural aspects of in-situ TiB reinforced Ti–6Al–4V composite processed by spark plasma sintering [J]. *Transactions of Nonferrous Metals Society of China*, 2015, 25(5): 1460–1467.
- [21] PARK S H, WOO K D, KIM S H, LEE S M, KIM J Y, KO H R, KIM S M. Mechanical properties and bio-compatibility of Ti–Nb–Zr–HA biomaterial fabricated by rapid sintering using HEMM powders [J]. *Korean Journal of Materials Research*, 2011, 21(7): 384–390. (in Korean)
- [22] KITSUGI T, NAKAMURA T, OKA M, YAN W Q, GOTO T, SHIBUYA T, KOKUBO T, MIYAJI S. Bone bonding behavior of titanium and its alloys when coated with titanium oxide (TiO₂) and titanium silicate (Ti₅Si₃) [J]. *Journal of Biomedical Materials Research*, 1996, 32(2): 149–156.
- [23] THIAN E S, LOH N H, KHOR K A, TOR S B. Microstructures and mechanical properties of powder injection molded Ti–6Al–4V/HA powder [J]. *Biomaterials*, 2002, 23(14): 2927–2938.
- [24] EVIS Z, USTA M, KUTBAY I. Hydroxyapatite and zirconia composites: Effect of MgO and MgF₂ on the stability of phases and sinterability [J]. *Materials Chemistry and Physics*, 2008, 110(1): 68–75.
- [25] LONG Y, ZHANG H Y, WANG T, HUANG X L, LI Y Y, WU J S, CHEN H B. High-strength Ti–6Al–4V with ultrafine-grained structure fabricated by high energy ball milling and spark plasma sintering [J]. *Materials Science and Engineering A*, 2013, 585: 408–414.
- [26] WANG Y M, HUANG J Y, JIAO T, ZHU Y T, HAMZA A V. Abnormal strain hardening in nanostructured titanium at high strain rates and large strains [J]. *Journal of Materials Science*, 2007, 42(5): 1751–1756.
- [27] CHU C, LIN P, DONG Y, XUE X, ZHU J, YIN Z. Fabrication and characterization of hydroxyapatite reinforced with 20 vol % Ti particles for use as hard tissue replacement [J]. *Journal of Materials Science: Materials in Medicine*, 2002, 13(10): 985–992.
- [28] LI Y H, YANG C, WANG F, ZHAO H D, QU S G, LI X Q, ZHANG W W, LI Y Y. Biomedical TiNbZrTaSi alloys designed by d-electron alloy design theory [J]. *Materials and Design*, 2015, 85: 7–13.
- [29] LI Y Y, ZOU L M, YANG C, LI Y H, LI L J. Ultrafine-grained Ti-based composites with high strength and low modulus fabricated by spark plasma sintering [J]. *Materials Science and Engineering A*, 2013, 560: 857–861.
- [30] ZHOU X, MOHANTY P. Electrochemical behavior of cold sprayed hydroxyapatite/titanium composite in Hanks’ solution [J]. *Electrochimica Acta*, 2012, 65: 134–140.

- [31] FONTANA M G. Corrosion engineering [M]. New York: McGraw-Hill, 1986. 438–440: 891–895.
- [32] ZHENG Y F, WANG B L, WANG J G, LI C, ZHAO L C. Corrosion behaviour of Ti–Nb–Sn shape memory alloys in different simulated body solutions [J]. Materials Science and Engineering A, 2006, 4867–4874.
- [33] CREMASCO A, OSÓRIO W R, FREIRE C M A, GARCIA A, CARAM R. Electrochemical corrosion behavior of a Ti–35Nb alloy for medical prostheses [J]. Electrochimica Acta, 2008, 53(14): 4867–4874.

放电等离子烧结 Ti-35Nb-7Zr-xHA 复合材料的力学性能与腐蚀性能

何正员¹, 张磊¹, 单文瑞¹, 张玉勤^{1,2}, 周荣¹, 蒋业华¹, 谭军^{1,3,4}

1. 昆明理工大学 材料科学与工程学院, 昆明 650093;
2. 云南省钛材应用产品工程技术研究中心, 昆明 650093;
3. Institute for Complex Materials, IFW Dresden, Dresden D-01171, Germany;
4. Institute of Materials Science, TU Dresden, Dresden D-01062, Germany

摘要: 为了改善 Ti–Nb–Zr 合金的生物活性, 采用放电等离子烧结(SPS)制备了 Ti–35Nb–7Zr–xHA(羟基磷灰石, $x=5, 10, 15, 20$, 质量分数, %)复合材料。借助 XRD、SEM、力学测试以及电化学测试手段研究了 HA 含量对复合材料显微组织、力学性能和腐蚀性能。结果表明, 所有复合材料的物相主要由 β -Ti 基体、 α -Ti 和金属–陶瓷相 (CaO, CaTiO₃, CaZrO₃, Ti_xP_y 等)组成, 此外, 含 15% HA 和 20% HA 的复合材料中出现了少量残余的 HA; 随着 HA 含量的增加, 复合材料的抗压强度均高于 1400 MPa, 复合材料(5%–15% HA)的弹性模量呈较小变化趋势 (46–52 GPa), 更加接近人骨的弹性模量。在 Hank's 溶液中的电化学试验表明, HA 含量为 15%时, 复合材料的钝化电流密度和腐蚀电流密度较低, 显示了较好的腐蚀性能。因此, Ti–35Nb–7Zr–15HA 复合材料可作为一种骨科植入手术中较好的替代材料。

关键词: 钛复合材料; 放电等离子烧结; 显微组织; 力学性能; 腐蚀性能

(Edited by Yun-bin HE)